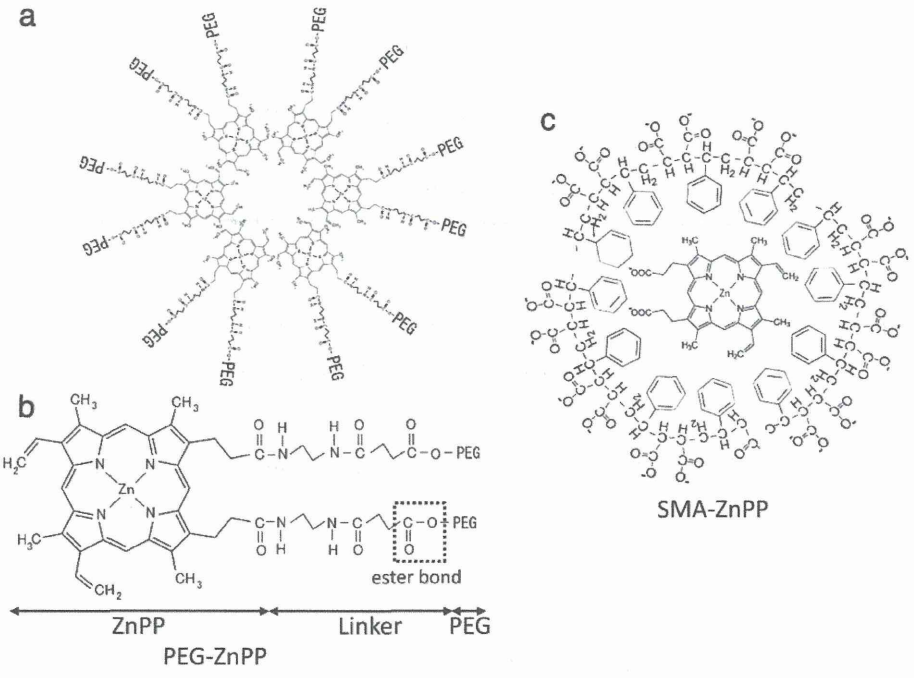

Fig. 1. In (a), hydrophobic ZnPP heads clustered and PEG chain tails with hydrophilic property extend outward direction in contact with water. (b) depicts each component of PEG-ZnPP (c) styrene residue of hydrophobic nature clustered and encapsulating ZnPP inside. Poly carboxylate groups and facing toward water.

molecules is the critical steps to exert cytotoxicity, since ZnPP is a competitive inhibitor of HO-1. Therefore its access to HO-1 molecules needs to be elucidated. In this study, we investigated the intracellular fate of PEG-ZnPP and SMA-ZnPP micelles focusing on the mode of internalization, subcellular localization and uncoating process of micelles. Different mechanisms of ZnPP release from each micelle were found to undergo at molecular level in the tissue and at the cellular levels.

2. Materials and methods

2.1. Materials

Protoporphyrin IX (PP) and antibiotics (penicillin and streptomycin) were obtained from Sigma Aldrich Chemical Co., St. Louis, MO. Free ZnPP was obtained from Frontier Scientific, Inc., Salt Lake, Utah. SMA (maleic anhydride form) (mean mol wt. ≈ 1600) was obtained from Kurary Co. Ltd., Kurashiki, Japan, which was used after hydrolysis in 0.1 M NaOH at 60 °C for 5 h. *N*-succinimidyl polyethylene glycol with a mean molecular weight of 2300 containing ester bond between PEG and N-succimide was obtained from NOF, Tokyo, Japan. RPMI-1640 medium and fetal bovine serum was obtained from GIBCO, Grand Island, NY. Primary antibody against human heme oxygenase-1 (HO-1) was obtained from Santa Cruz Biotechnology, Inc., CA. FITC-labeled goat anti-rabbit IgG labeled with FITC was obtained from Biomedical Technologies, Inc., MA. Ethylenediamine and other chemicals were reagent grade commercially available.

2.2. Synthesis of ZnPP and SMA-ZnPP

ZnPP and SMA-ZnPP was prepared according to the method as described by Iyer et al. previously [11]. Briefly hydrolysed SMA (cSMA) was dissolved at concentration of 10 mg/ml in deionized water and pH was adjusted to 10.5 with 0.1 M NaOH. ZnPP solution at 5 mg/ml in DMSO was added to cSMA solution under stirring for 1 h. Then the pH was adjusted slowly to pH 3.0 using 0.1 M HCl at 20 °C resulting in precipitation of SMA-ZnPP micelles. Precipitates were collected by centrifugation and were washed with cold deionized water thrice. The precipitates were resuspended in deionized water and pH was adjusted to 7.4 with 0.1 M NaOH to obtain clear solution of SMA-ZnPP. Finally ultrafiltration using the Millipore Lab Scale TFF system (Millipore, Bedford, MA) with a membrane cut-off MW of 10 kDa under a pressure of about 0.7 kg/cm^2 was carried out to remove low MW components including excess free cSMA and concentrate the SMA-ZnPP micelles to 1/10 volume, of which process was repeated three times at 4 °C. Then, the concentrate was lyophilized to obtain fluffy deep brownish powder. Finally obtained SMA-ZnPP contains 35 w/w% of ZnPP in its micellar structure.

2.3. Synthesis of PEG-ZnPP

PEG-ZnPP micelles were prepared according to the method described by Sahoo et al. with some modification [9]. Briefly carboxyl group of PP (100 mg in 20 mL of tetrahydrofran) was reacted with ethylenediamine (2.4 mL) to introduce two functional amino groups via amide bond to PP. The obtained product, *bis*-(diaminoethyl) protoporphyrin (PPED) was absorbed onto the activated alumina and washed with chloroform five times. Then PPED was eluted with chloroform containing 5% ethylenediamine. And then polyethylene glycol (mean Mw of 2300) with succinimide (54 mg) was reacted to PPED (5 mg). Obtained pegylated protoporphyrin (PEG-PP) was applied to aluminum oxide column (2.5 cm × 10 cm) equilibrated with chloroform and eluted with chloroform to remove unreacted PPED. Then 100 M excess of zinc acetate was added to PEG-PP with stirring and zinc was chelated for 2 h to achieve PEG-ZnPP. PEG-ZnPP was transferred to water followed by Amicon® ultra filtration system with 10 kDa cut off membrane under pressure condition (0.2 MPa) to remove unreacted PEG and excess zinc acetate. Product showed a single peak on HPLC using column of Asahipack GF310-HQ (solvent system: 70% methanol, 30% DMSO and 0.001% trifluoroacetic acid).

2.4. Cell culture

Human chronic myeloid leukemia cell lines (K562) were cultured in RPMI 1640 with 10% fetal bovine serum at 37 °C under the atmosphere of 5% CO_2-95% air.

2.5. Quantification of ZnPP in cells

K562 cells were placed in 12-well plate (5×10^5 cells/well). After overnight pre-incubation, cells were treated with ZnPP, SMA-ZnPP or PEG-ZnPP for indicated time at the concentrations shown in the figure legend. Free ZnPP was dissolved in DMSO, other micellar ZnPP was dissolved in PBS (pH 7.4). After incubation for given times, cells were collected by centrifugation and washed with PBS thrice at 4 °C. Then cells were sonicated (30 W, 30 s, Dr.Hielscher, UP50H homogenizer, tip drip type) in ethanol at ice chilled condition (0 °C) followed by centrifugation to collect supernatant containing ZnPP, and fluorescence intensity (excitation at 420 nm, emission at 598 nm) of the ethanol extract was measured.

2.6. Subcellular localization of ZnPP micelles

Subcellular localization of SMA-ZnPP was analyzed by Nikon Eclipse TE2000-E Confocal Microscope (Nikon, Japan). K562 cells were cultured in RPMI medium with 10% FCS without phenol red in 35 mm (Ø) glass bottom dish (Matsunami glass, Osaka, Japan). Cells were treated with 30 μM of ZnPP, SMA-ZnPP or PEG ZnPP for indicated time at 4 °C or 37 °C. ZnPP, SMA-ZnPP and PEG-ZnPP were excited by 488 nm and detected through the 565–615 nm band path filter. To investigate the colocalization of ZnPP derivatives at ER compartment, 3,3′-dihexyloxacarbocyanine iodide (DIOC6) was used for a staining of ER (endoplasmic reticulum). DIOC6 was excited at 488 nm and detected through the 500–530 nm band path filter. In this experiment, ZnPP and SMA-ZnPP were excited at 543 nm and were visualized by 565–615 nm band path filter to avoid a bleed from a fluorescence of DIOC6.

2.7. Immunofluorescence staining

K562 cells treated with ZnPP or SMA-ZnPP for 3 h were collected by centrifugation (1000 rpm, 5 min, 4 °C) and washed with PBS thrice. The cells were fixed with 4% paraformaldehyde at room temperature for 10 min following washing twice with PBS containing 10 mM glycine. Then the cells were made permeable with 0.1% Triton X-100 for 10 min at room temperature and washed with PBS thrice, followed by treatment with 3% BSA in PBS at room temperature for 30 min to react excess remaining paraformaldehyde and then washed thrice for 5 min in PBS. The cells were then incubated with primary rabbit antibody against human HO-1 (diluted 1:100 in 3% BSA) at room temperature for 1 h. After washing with PBS thrice, the cells were incubated with FITC-labeled goat anti-rabbit IgG (diluted 1:1000) at 25 °C for 1 h and then again washed thrice for 10 min in PBS. Then cells were resuspended in PBS, and examined under a confocal microscope. Both FITC-labeled goat anti-rabbit IgG and ZnPP was excited at 488 nm and detected through a 485–530 nm band path filter and a 565–615 nm band path filter respectively.

2.8. Analysis of mechanism of intracellular uptake of ZnPP micells into cells

The cells were seeded in 12-well culture plates at a density of 2×10^5 per well, and incubated at 4 °C, or at 37 °C for indicated time period with or without various inhibitors of endocytosis for 1 h prior to the addition of ZnPP, SMA-ZnPP or PEG-ZnPP. After incubation, the cells were harvested by centrifugation at 700 rpm and washed with PBS thrice at room temperature followed immediately by flow cytometry analysis (FACSCalibur, Becton Dickinson and Co.). About 1×10^4 cells were collected, and the mean fluorescence intensity was recorded and analyzed for each sample.

2.9. Disintegration study of SMA-ZnPP in cell free system

SMA-ZnPP micelle (4 μg/mL) was incubated with sodium dodecyl sulfate, soybean lecithin (wako) or rat liver microsome fraction at 25 °C. Disintegration of SMA-ZnPP was also examined in 50 mM phosphate buffer (pH7.5) or 20 mM citrate buffer (pH5.0) with 150 μg/mL of lecithin. At the indicated time period, incubates were excited at 420 nm and fluorescent intensity at 599 nm was measured by fluorescent spectrometer.

2.10. HPLC analysis of intracellular PEG-ZnPP and HO-1 inhibitory assay

K562 cells were treated with 30 μM of PEG-ZnPP for 5 h, and then cells were washed with PBS thrice, followed by extraction of intracellular PEG-ZnPP with ethanol. The extracted PEG-ZnPP was then subjected to HPLC analyses with an Asahipak GF-310 HQ column (7.5 mm × 300 mm). The mobile phase consisted of 70% methanol, 30% dimethyl sulfoxide and 0.001% of trifluoroacetic acid at a flow-rate of 0.8 mL/min. Elutes was detected at 415 nm of ZnPP. HO-1 inhibitory activity of PEG-ZnPP was performed as described previously [9]. Briefly, PEG-ZnPP derivatives were incubated with rat liver cytosolic fraction (1.0 mg/mL of protein) in 100 mM phosphate buffer (pH7.4) for 30 min at 25 °C. Then rat splenic microsomal fraction (1.0 mg/mL of protein), 333 μM nicotinamide adenine dinucleotide phosphate (NADPH) and 33 μM of hemin was added to initiate the reaction. The reaction mixture was incubated for 30 min at 37 °C. The bilirubin formed in the reaction was extracted with 1.0 mL of chloroform, and the bilirubin concentration was determined spectroscopically by the difference in absorbance at 465 nm and 530 nm.

3. Result

3.1. Intracellular behavior of SMA-ZnPP and PEG-ZnPP

Protoporphyrin IX (PP) itself does not inhibit HO-1 enzymatic activity, however, the zinc coordination with protoporphyrin IX (ZnPP) becomes inhibitor for HO-1 activity. The Ki value is almost the same among ZnPP, SMA-ZnPP and PEG-ZnPP [9,11]. Protoporphyrin IX has an absorption max (λ_{max}) of 406 nm and exhibit single fluorescence emission peak at 641.5 nm in ethanol, while that of authentic ZnPP has λ_{max} 422.5 nm and fluorescent max at 598.5 nm with a minor shoulder approximately at 650 nm in ethanol. To quantify the ZnPP derivatives in the cells, it was extracted by 95% ethanol and fluorescent spectrum was examined. As shown in Fig. 2, intracellular ZnPP showed fluorescence emission peak at 598.5 nm which is consistent with that of authentic ZnPP. SMA-ZnPP and PEG-ZnPP also showed fluorescent spectrum which is consistent to that of ZnPP.

3.2. Intracellular uptake and subcellular localization of ZnPP micelles

Fluorescent intensity of ZnPP derivatives will change by its conformational states. In water solution, both ZnPP derivatives form micellar structure and its fluorescence is quenched. Its fluorescence is recovered by addition of EtOH (Fig. 3a). However its fluorescence quenching of PEG-ZnPP in water solution is weaker than that of SMA-ZnPP, probably due to the different micellar structure of these two compounds. To quantify the amount of ZnPP derivatives by fluorescent intensity, we checked fluorescent efficiency of ZnPP, SMA-ZnPP and PEG-ZnPP in ethanol, in which all micelles are disrupted and emit fluorescence. The concentration of ZnPP derivatives was standardized as ZnPP equivalent concentration by absorbance at 420 nm. Three ZnPP derivatives showed comparable fluorescent intensity under micelle disrupting condition in ethanol (Fig. 3b). To examine the cellular

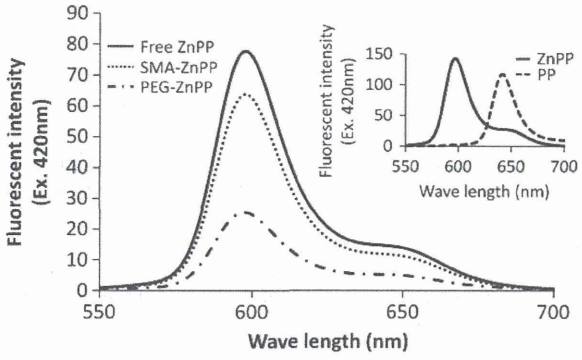

Fig. 2. Fluorescent spectra of ZnPP (solid line), SMA-ZnPP (dashed line) and PEG-ZnPP (dash–dot line) of extracts from the treated cells. K562 cells were treated with 20 μM of ZnPP, SMA-ZnPP and PEG-ZnPP for 5 h. After incubation, fluorescent spectra of intracellular ZnPP, SMA-ZnPP and PEG-ZnPP were recorded as described in Materials and methods. Inset shows the fluorescent spectra of protoporphyrin IX (PP) (dashed line) and ZnPP (solid line) in ethanol.

internalization of ZnPP and both types of ZnPP micelles, K562 cells were incubated with them for indicated time. Intracellular ZnPP was extracted with ethanol and quantified by fluorescence intensity of ZnPP itself (Ex. 420 nm and Em. 590 nm). As shown in Fig. 3, ZnPP and both ZnPP micelles were incorporated into the cells in a time dependent manner. More interestingly, uptake of SMA-ZnPP into the cells was about 2.5 times more efficiently than PEG-ZnPP at 300 min incubation.

Intracellular localization of ZnPP and ZnPP micelles were also examined under the fluorescent confocal laser microscopy. Confocal laser microscopy imaging showed that ZnPP and both ZnPP micelles accumulated at the cellular membrane at first and then gradually accumulated more distinctly at the perinuclear site after 30 min or later (Fig. 4). ZnPP is highly hydrophobic and is predicted to be associated with hydrophobic compartment in the cell. Thus we first examined the possibility of localization of free ZnPP and SMA-ZnPP micelles at the endoplasmic reticulum (ER); for that purpose we performed double staining with a DIOC6 which accumulates in the ER and emits fluorescence at the ER (Fig. 5a). As shown in Fig. 5a, ZnPP and both ZnPP micelles colocalized with DIOC6 suggesting localization of free ZnPP and ZnPP micelles in the ER. Because heme oxygenase-1 (HO-1) is found mainly at the ER as stained with antibody against HO-1, we hypothesized that ZnPP and SMA-ZnPP colocalized with HO-1. As expected, ZnPP and SMA-ZnPP showed clear colocalization with HO-1 protein when ZnPP or SMA-ZnPP was added to K562 cells (Fig. 5b).

3.3. Mode of intracellular uptake of ZnPP and ZnPP micelles; endocytosis

To evaluate the mechanism of intracellular uptake of ZnPP and ZnPP micelles, K562 cells were incubated with 20 μM each of ZnPP, SMA-ZnPP and PEG-ZnPP respectively at 4 °C or 37 °C for 2 h. As shown in Fig. 6, ZnPP and ZnPP micelles were taken up into the cells efficiently at 37 °C during incubation, however, intracellular uptake of free ZnPP and SMA-ZnPP micelles were suppressed to a great extent at 4 °C as revealed by FACS analysis (Fig. 6b). Further, compared to the strong staining of ZnPP, SMA-ZnPP or PEG-ZnPP micelles in cells at 37 °C, they showed no or quite faint staining only at a cellular membrane when incubated at 4 °C (Fig. 6). In addition, as shown in Fig. 7, internalization of ZnPP was inhibited by macropinocytosis

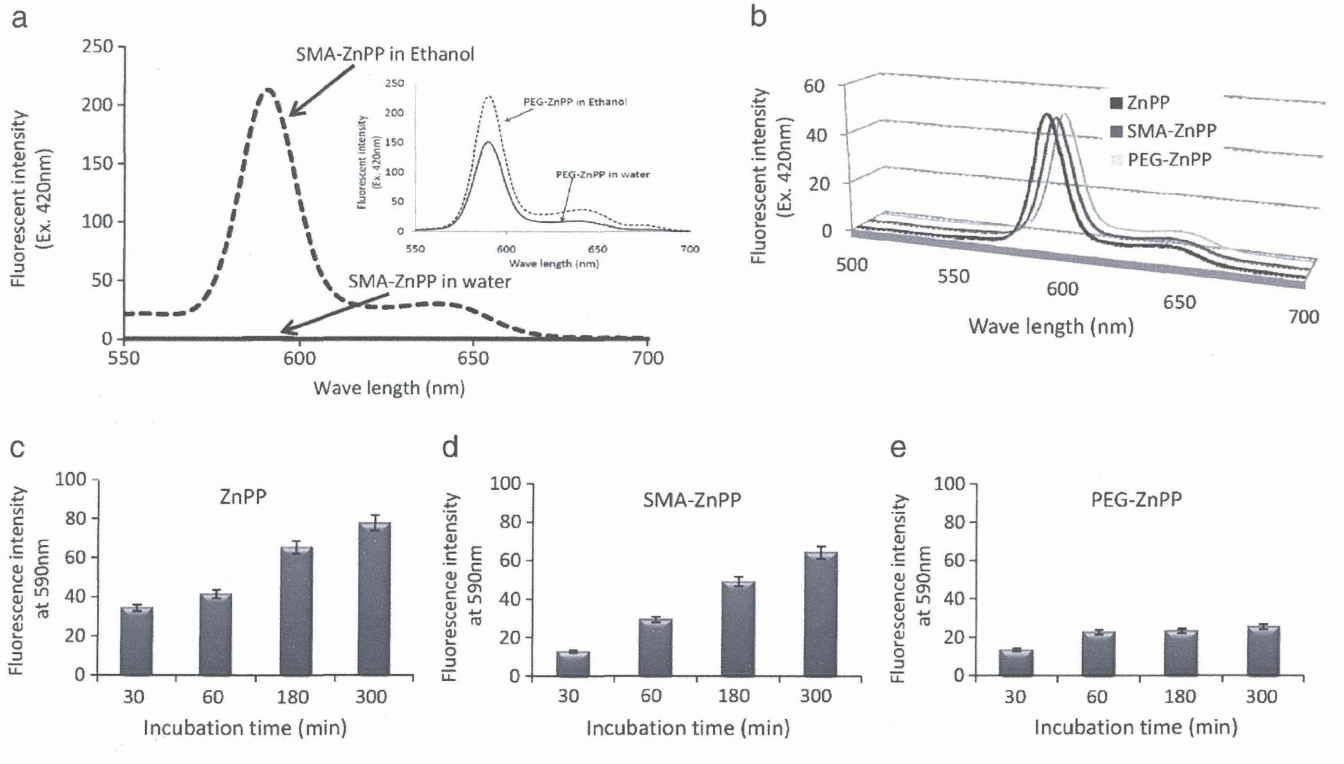

Fig. 3. Intracellular uptake of ZnPP derivatives as quantified by fluorescence intensity after extraction of ZnPP. (a) SMA-ZnPP (4 μg/mL) or PEG-ZnPP (14ug/mL) was dissolved in distilled water or ethanol, which was excited at 420 nm and fluorescent spectrum was recorded by fluorescent spectrometer. (b) 0.25 μM ZnPP equivalent of ZnPP, SMA-ZnPP and PEG-ZnPP in ethanol was excited at 422 nm and fluorescent spectra were recorded. K562 cells in suspension culture were treated with 20 μM of (c) free ZnPP, (d) SMA-ZnPP and (e) PEG-ZnPP for period of indicated time. After incubation, the cells were washed with PBS and the amount of intracellular ZnPP and SMA-ZnPP and PEG-ZnPP were determined after extraction by ethanol as described in Materials and methods.

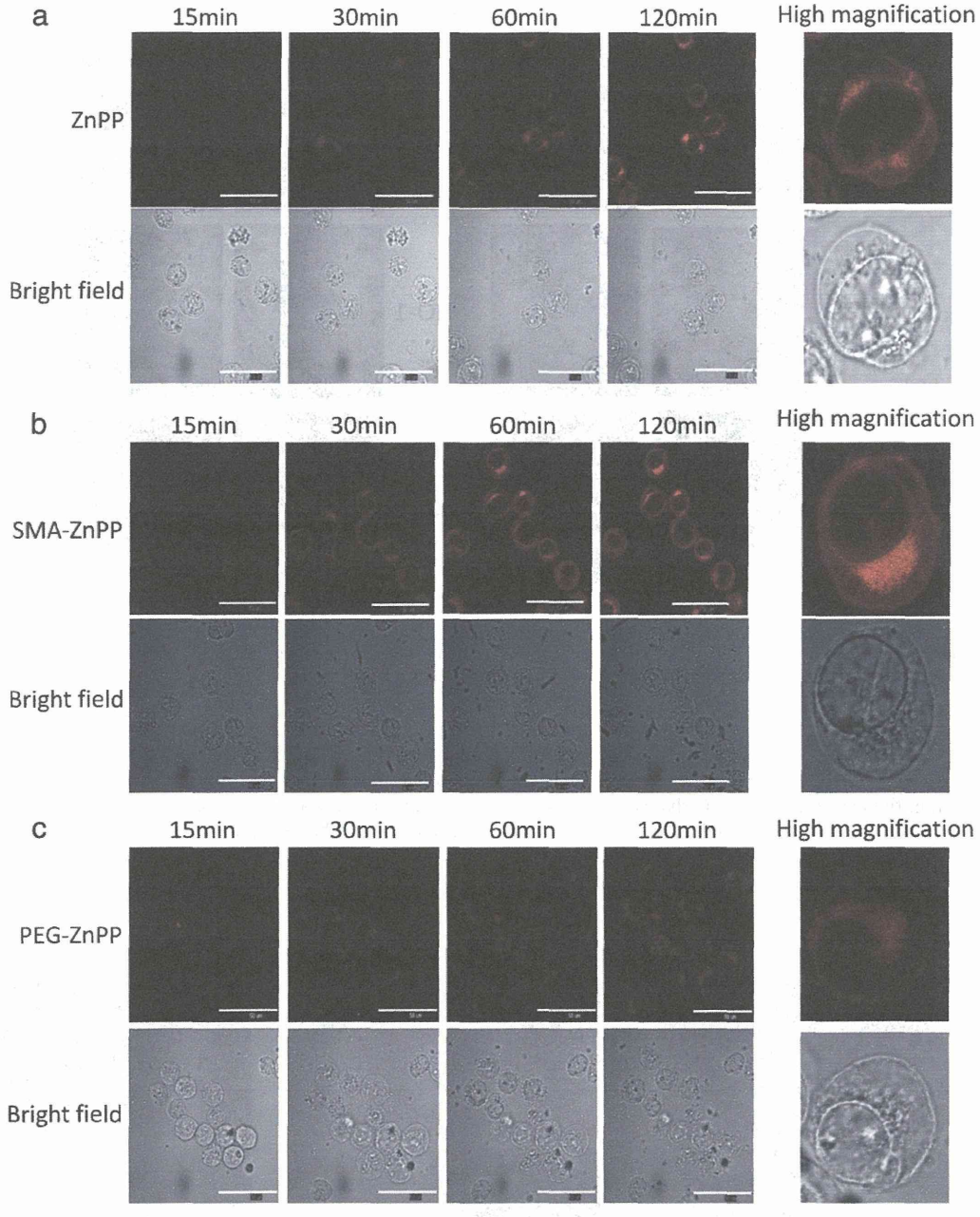

Fig. 4. Confocal fluorescence microscopy of K562 cells treated with 30 μM of (a) ZnPP, (b) SMA-ZnPP and (c) PEG-ZnPP. K562 cells were grown on glass bottom dish to logarithmic phase, incubated with 30 μM of ZnPP, SMA-ZnPP and PEG-ZnPP at 37 °C for indicated time. Cells were then taken for microscopic observation. Red color indicates the fluorescence of ZnPP. Scale bar shows 50 μm length.

inhibitor, amiloride. Pretreatment with sucrose and colchicine suppressed uptake of SMA-ZnPP, similarly intracellular uptake of PEG-ZnPP was suppressed by sucrose treatment (Fig. 7).

3.4. Disintegration of SMA-ZnPP micelles by amphiphilic components of cells

In the SMA-ZnPP micelles, SMA is thought to form a shell of micelle where ZnPP is encapsulated inside of the micelles, which is believed to be liberated eventually for its action. Therefore, disruption of SMA-ZnPP micelles followed by liberation of ZnPP is a crucial step to exert the pharmacological effect to inhibit HO-1 enzyme activity in the cells. To examine this possibility of disruption of SMA-ZnPP micelles in cells, we carried out a model experiment, in that SMA-ZnPP was incubated with soybean lecithin which mimics the cellular membrane components, phosphatidylcholine. As shown in Fig. 8, SMA-ZnPP does not emit fluorescence in water solution and exhibits fluorescence when ZnPP is liberated from the micelles as disrupted by ethanol or 10% SDS [11]. Coincubation with increasing amount of lecithin or SDS indeed resulted in increased fluorescence emission from free ZnPP. Vehicle alone has no effect on fluorescence increament of SZP (Fig. 8a). Time dependent increase of fluorescence emission was also seen when incubated with soybean lecithin. Fig. 8b also shows that SMA micelle disruption with lecithin proceeds rapidly at the condition of pH 7.5 than pH 5.5. Similar results were obtained when it was incubated with mouse liver microsomal fraction which contains membrane components (Fig. 8c).

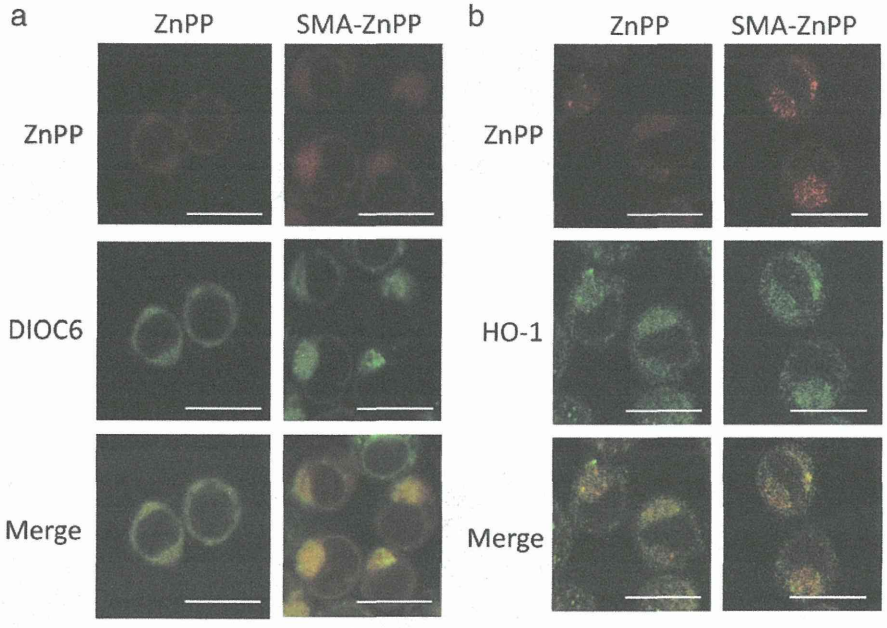

Fig. 5. Subcellular localization of ZnPP micelles. (a) shows the ER localization of ZnPP micelles. ZnPP micelles (red) and DIOC6 (green) were visualized by confocal laser microscopy. (b) shows the colocalization of ZnPP micelles (red) with HO-1 (green). Cells were grown to logarithmic phase, incubated with 30 μM of ZnPP and SMA-ZnPP for 2 h. ER was stained by DIOC6 and HO-1 was visualized with FITC-conjugated to anti-rabbit IgG. Scale bar shows 20 μm in length.

3.5. Liberation of free ZnPP from PEG-ZnPP

As shown in Fig. 1, in the PEG-ZnPP, two PEG chains are covalently linked to the spacer ethylenediamine that is conjugated to the carboxyl group of protoporphyrin IX. ZnPP is a competitive inhibitor of HO-1 thus PEG-cleavage might be critical step to exert HO-1 inhibitory activity. We next examined the intracellular processing of PEG-ZnPP by HPLC analyses. K562 cells were treated with PEG-ZnPP for 5 h at 37 °C in RPMI medium and intracellular PEG-ZnPP or its hydrolysed products was extracted by ethanol followed by HPLC analyses. As shown in Fig. 9, parental PEG-ZnPP had a retention time at 6.3 min and intracellular PEG-ZnPP after incubation with cells and extraction showed delayed

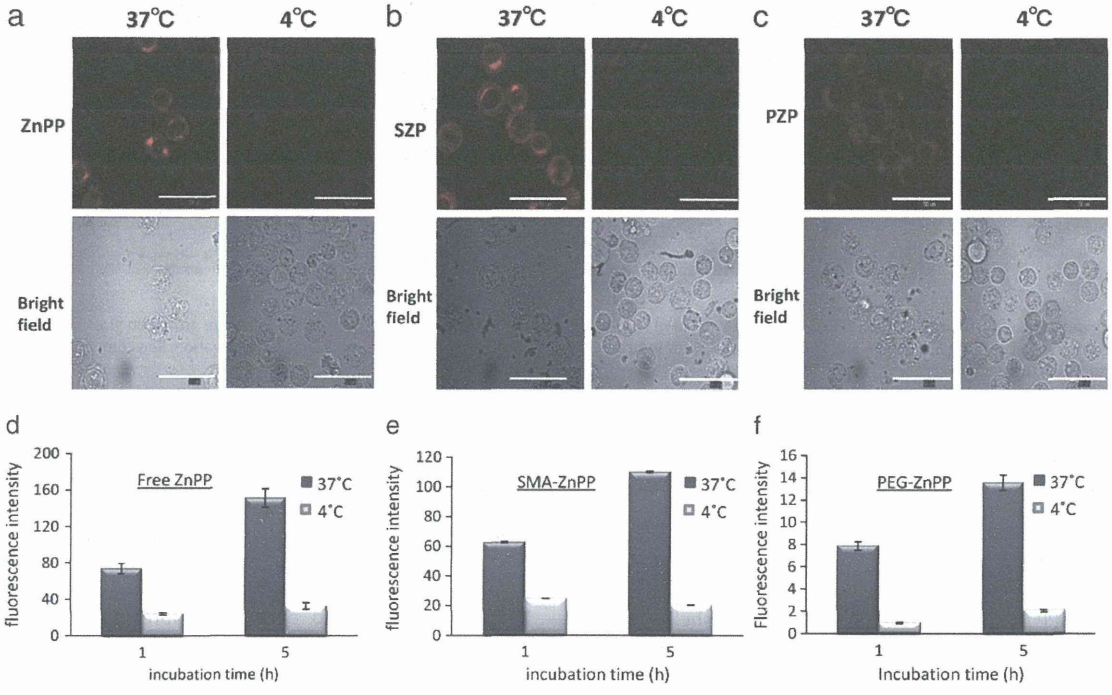

Fig. 6. Intracellular uptake of ZnPP micelles at different temperature. Intracellular ZnPP (red) in K562 cells treated with 20 μM of (a) ZnPP, (b) SMA-ZnPP and (c) PEG-ZnPP for 2 h at 37 °C (left panel) and at 4 °C (right panel) were visualized by confocal laser microscopy. Amount of ZnPP in K562 cells treated with (d) ZnPP, (e) SMA-ZnPP and (f) PEG-ZnPP were quantified by FACS analysis.

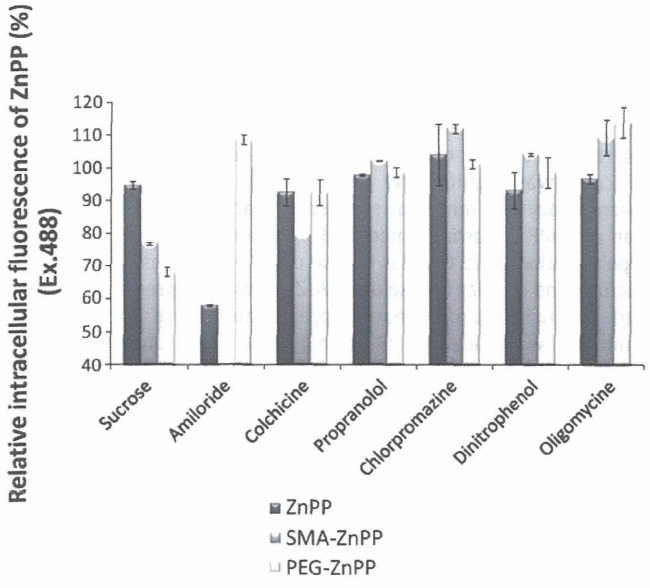

Fig. 7. Inhibition of intracellular uptake of ZnPP micelles by endocytosis inhibitors. K562 cells were treated with ZnPP (black column), SMA-ZnPP (gray column) and PEG-ZnPP (white column) with or without indicated endocytosis inhibitors. Cells were preincubated with these inhibitors for 60 min prior to addition of ZnPP micelles. Intracellular amount of ZnPP was quantified by FACS analysis.

retention time at 7.1 min indicating the processing of PEG-ZnPP in cells or cell periphery (Fig. 9a). Furthermore this cleaved PEG-ZnPP was also found to have HO-1 inhibitory activity (Fig. 9b).

4. Discussion

The most important properties for anticancer drugs are summerized as follows; (i) selective accumulation of the drugs in the tumor tissue, (ii) efficient intracellular uptake, and (iii) access of active component to the intracellular target molecules. To confer these properties to the candidate drugs, a numbers of methods may be possible. One of the most universal tumor selective targeting is based on the EPR (enhanced permeability and retention) mechanism dependent selective targeting, in which macromolecular formulations are preferred. The first such example is the conjugation of SMA and proteinaceous drug neocarzinostatin (NCS) resulting SMANCS [15,26–28]. For this purpose, encapsulation of the low molecular weight drugs into the micelles or liposome, or conjugation to polymeric carriers such as SMA, HPMA (N-(2-hydroxypropyl)methacrylamide), PEG or other block copolymers with biocompatible and carrier properties. These methods can improve the physicochemical and pharmacokinetic properties of low MW drugs, or various proteins [15,18,29–31].

Both PEG-ZnPP and SMA-ZnPP exhibit micellar property and have molecular weight of about 140 kDa and 90 kDa respectively and mean size distribution about 180 nm and 50 nm respectively. Both PEG-ZnPP and SMA-ZnPP showed high water solubility and accumulate more selectively in the tumor tissue, and they exert potent anti-tumor activity when injected i.v. [8,11].

Although we have characterized in vivo body distribution and anti-tumor effect of both PEG-ZnPP and SMA-ZnPP, mechanism of cellular uptake and intracellular localization remained to be clarified. For this reason, mechanism of cellular uptake and intracellular fate of these micelles were investigated. Very recently, we have reported that growth or DNA synthesis of human chronic myeloid leukemia (CML) derived cell line K562 cells were suppressd by PEG-ZnPP and SMA-ZnPP [7]. In the present study, we report that both PEG-ZnPP and SMA-ZnPP were internalized in K562 cells at different rate. Fluorescent intensity of ZnPP

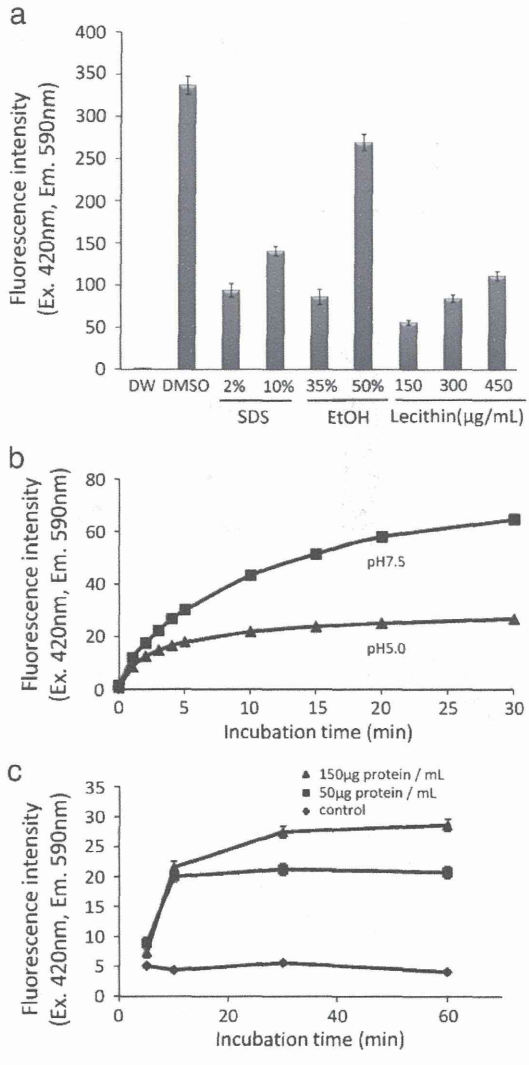

Fig. 8. Stability analysis of SMA-ZnPP and effect of various amphiphilic agents for bursting of micelles. (a) Fluorescence intensity of SMA-ZnPP incubated with different concentration of lecithin for 30 min or SDS for 15 min was measured by fluorescent spectroscopy. (b) Fluorescence intensity of SMA-ZnPP was measured as the micelles were incubated with lecithin at pH 7.5 (square) or pH 5.5 (triangle). (c) Fluorescence intensity of SMA-ZnPP incubated with 150 μg/ml (triangle) and 50 μg/ml (square) of mouse liver microsomal fraction for indicated time.

derivatives is highly dependent on its conformational states, π–π stacked form or dispersed free form. Compact molecular packing of ZnPP in SMA micelles quenched fluorescence perhaps by π–π stacking or energy transfer (Figs. 3a and 8). Thus it may be difficult to compare among the intracellular amounts of three ZnPP derivatives by fluorescent intensity such as flowcytometry due to possible quenching (Fig. 6). In the organic solvent such as ethanol, in which ZnPP derivatives are dispersed states, three ZnPP derivatives showed comparable fluorescent intensity (Fig. 3a). This result indicates that fluorescent intensity in ethanol correlates with ZnPP amount of the ZnPP derivatives. Thus we extracted intracellular ZnPP derivatives in ethanol to represent the realistic amount of ZnPP, SMA-ZnPP and PEG-ZnPP in cells. SMA-ZnPP is about 2.5 times more rapidly internalized into the cells than PEG-ZnPP at 300 min (Fig. 3). Increment of uptake when compared from 30 min to 300 min of SMA-ZnPP is 5 times more than PEG-ZnPP (Fig. 3). FACS analysis also supports the faster uptake of SMA-ZnPP; intracellular fluorescent intensity of SMA-ZnPP was 7 times higher than that of PEG-ZnPP at 5 h (Fig. 6). This suppressed uptake of

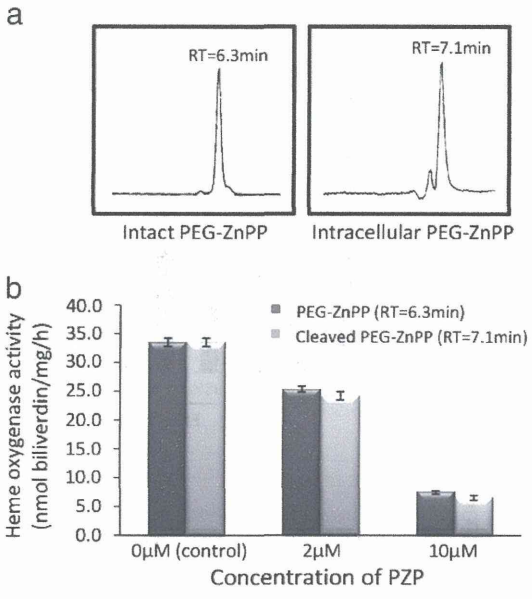

Fig. 9. Intracellular processing of PEG-ZnPP. (a) Shows HPLC analysis of intact PEG-ZnPP (left panel), PEG-ZnPP (right panel). (b) Shows HO-1 inhibitory activity of intact PEG-ZnPP (black column) and cleaved PEG-ZnPP (gray column). Both PEG-ZnPP were preincubated with mouse liver cytosol and spleen microsome for 30 min at 25 °C prior to addition of hemin as a substrate of HO-1 enzyme reaction. HO-1 activity was measured as described in the text.

PEG-ZnPP may be caused by the fact that hydrated PEG-layer of the PEG micelles interferes the interaction with receptor site on the cell surface that is involved in endocytotic uptake of micelles. This suppressed intracellular uptake is named PEG-dilemma [32,33]. Meanwhile, intracellular uptake of SMA-ZnPP was very active and almost comparable to that of free ZnPP. This may be due to the affinity between the hydrophobic residue of SMA and surface receptor. Free ZnPP is internalized most rapidly among the three tested ZnPP derivatives. Nevertheless free ZnPP is poorly water soluble and thus difficult for clinical application, and more important, as small molecule it may disappear from the circulation so rapidly that it never shows EPR effect for tumor delivery. Namely, PEG and SMA based micelle formulation gives high water solubility and improved pharmacokinetic property including high plasma concentration and antitumor activity of ZnPP. However, PEG-ZnPP showed much less efficient cell uptake. As a result PEG-ZnPP exhibited less cytotoxic activity in the in vitro setting compared to free ZnPP or SMA-ZnPP (data not shown). Whereas SMA micelles confer the micellar capacity for efficient cell uptake as reported for SMANCS [34,35].

Cell membrane forms a barrier impermeable to large molecules above about 1 kDa. However, cells are equipped with active transport systems across the cell membrane called endocytosis for most macromolecules such as micelles, liposomes, antibody and DNA/RNA complex. Endocytotic cellular uptake is believed to be more active in dividing cells such as tumor cells than non-dividing normal cells. Previously, SMANCS was shown to undergo endocytotic pathway for its antitumor activity. Namely SMANCS is rapidly internalized into the cells [34,35]. Many other macromolecular drugs such as liposomes and HPMA conjugated drugs also show endocytotic cellular internalization [20–22].

In this study we showed that free ZnPP, SMA-ZnPP micelle and PEG-ZnPP conjugate were internalized by endocytotic pathway. It is considered that at low temperature (below 20 °C), endocytotic uptake of macromolecules was suppressed probably due to suppressed ATP generation by oxidative phosphorylation. Thus suppressed internalization at low temperature (4 °C) and rapid uptake at 37 °C indicate that endocytosis is the major mechanism of cellular drug uptake (Fig. 6). In addition, it should be noted that in this study, the fluorescent intensity of ZnPP, SMA-ZnPP and PEG-ZnPP is directly detected by flowcytometry, not through ethanol extraction method, because of the difference of fluorescent efficiency of ZnPP and derivatives as discussed above, it is difficult to compare the internalized amount of SMA-ZnPP and PEG-ZnPP. Intracellular uptake of ZnPP was significantly inhibited by amiloride, which is a macropinocytosis inhibitor, suggesting that the cellular internalization of ZnPP is partially mediated by macropinocytotic pathway, a type of endocytosis. Cellular uptake of PEG-ZnPP was suppressed by sucrose, and cellular uptake of SMA-ZnPP was suppressed by sucrose and colchicine. Unfortunately precipitates were formed when amiloride was added to SMA-ZnPP that made analysis difficult. These results suggest that PEG-ZnPP is internalized by clathrin dependent endocytosis, whereas SMA-ZnPP is internalized not only by clathrin dependent endocytosis but also probably via microtubule dependent endocytosis mechanism. It seems that several different pathways may be involved in internalization of ZnPP, SMA-ZnPP and PEG-ZnPP. Further investigations are needed to clarify this point.

Protoporphyrin IX (PP) itself doesn't have HO-1 inhibitory effect or cytotoxicity as previously shown. However, ZnPP and both ZnPP micelles were shown to inhibit HO-1 in the cell [8,9], and cells treated with ZnPP and both ZnPP micelles showed the fluorescence spectrum corresponding to free ZnPP, the zinc coordinated form of protoporphyrin IX. This result suggests that after the internalization, both ZnPP micelles still exist as zinc in the tetrapyrrole, an active HO-1 inhibition form of Zn-protoporphyrin IX.

Fluorescence microscopy under a confocal laser microscope, based on the fluorescence of ZnPP was carried out in this study. As shown in Fig. 8, SMA-ZnPP micelle was shown to exhibit less fluorescence compared with free ZnPP in test tube as it was expected so because the fluorescence of SMA-ZnPP was quenched due to π–π interaction in the packed micelle. However, we found fluorescence of ZnPP micelles appeared eventually in the cells, indicating free ZnPP was released from the micelle to exhibit fluorescence. Namely, these results suggested that unique fate of SMA-ZnPP micelles being uncoated in the cells. Moreover as shown in Fig. 4a and b, fluorescence by SMA-ZnPP was found at cellular membrane as well as ER compartment after treatment for first 15 min–120 min. In contrast, PEG-ZnPP (Fig. 4c) showed very weak fluorescence at the ER compartment after the same time. HO-1 was also localized at the ER, colocalization with the fluorescence of ZnPP (see Fig. 5 merge). These results are consistent with an interpretation that ZnPP micelles exert cytotoxic activity through inhibiting to the HO-1 enzyme as free ZnPP.

ZnPP is thought to be tightly packed in the center core of SMA-ZnPP micelles (Fig. 1) as judged by quenching of its fluorescence and emergence of fluorescence upon disruption of the micelles (Fig. 2), suggesting that the liberation of free ZnPP from SMA-ZnPP micelle is needed to exert HO-1 inhibitory activity. Recently, Regehly et al. reported that SMA-ZnPP micelles exist as a free ZnPP-form in the cells and seem to be associated with hydrophobic environment such as lipid bilayer of cellular compartment, the data based on flash photolysis measurement of singlet oxygen [36]. Consistent with this previous report, release of free ZnPP may be brought about by micelle disintegration in the cells caused by the amphiphilic components in cells, particularly cell membrane such as phosphatidyl choline. We therefore examined this process of the ZnPP release in vitro from its SMA-ZnPP micelle with lecithin and microsomal membrane fraction, which was obtained from the tissue homogenate followed by ultracentrifugation at 100,000 g ppt (precipitate). Release of ZnPP was more rapid at pH 7.5 than pH 5.5. These observations suggest that disruption of SMA-ZnPP micelles proceeds in the presence of membrane component of cells as well as binding to lipophilic compartments in the cell such as ER compartment.

Recently Huan et al. synthesized PEG-lipid derivatives linked via ester linkage, ether linkage and amide linkage respectively. They

showed that PEG-lipid linked via ester linkage is most susceptible to PEG cleavage [37]. We also confirmed that PEG-ZnPP linked via ether linkage was more stable than PEG-ZnPP conjugated via ester linkage, and cleavage of ester linkage was accelerated by serum component (unpublished data). Along this line we clarified that PEG-ZnPP containing ester linkage is cleaved intracellularly (Fig. 9a). These findings suggest that ester linkage between PEG and ZnPP is the cleavable site by enzyme dependent or independent hydrolytic mechanisms (Fig. 1a). After cleavage of PEG-ZnPP still have HO-1 inhibition activity (Fig. 9b).

In conclusion, we demonstrated here the uptake of different micelle preparations of ZnPP and their fate in the cells. SMA-ZnPP is internalized into cells much more rapidly than PEG-ZnPP by endocytotic pathway, followed by release of free ZnPP in the presence of membrane components. ZnPP is mainly colocalized with HO-1 at ER compartment and inhibits HO-1 activity which leads to higher oxystress then cell death. PEG-ZnPP is also internalized in cells slowly by endocytotic pathway and subjected of hydrolytic cleavage by either protease or esterase inside of, or in the vicinity of, the cells. PEG-ZnPP also shows colocalization with HO-1 and inhibits the HO-1 activity perhaps after the cleavage of PEG bond.

References

[1] S. Ishizawa, T. Yoshida, G. Kikuchi, Induction of heme oxygenase in rat liver. Increase of the specific mRNA by treatment with various chemicals and immunological identity of the enzymes in various tissues as well as the induced enzymes, J. Biol. Chem. 258 (7) (1983) 4220–4225.

[2] R.K. Kutty, M.D. Maines, Effects of induction of heme oxygenase by cobalt and tin on the in vivo degradation of myoglobin, Biochem. Pharmacol. 33 (18) (1984) 2924–2926.

[3] T.J. Smith, S. Haque, G.S. Drummond, Induction of heme oxygenase mRNA by cobalt protoporphyrin in rat liver, Biochim. Biophys. Acta 1073 (1) (1991) 221–224.

[4] K. Doi, T. Akaike, S. Fujii, S. Tanaka, N. Ikebe, T. Beppu, S. Shibahara, M. Ogawa, H. Maeda, Induction of haem oxygenase-1 nitric oxide and ischaemia in experimental solid tumours and implications for tumour growth, Br. J. Cancer 80 (12) (1999) 1945–1954.

[5] J.H. Kaplan, J.N. Groves, Liver and blood cell catalase activity of tumor-bearing mice, Cancer Res. 32 (6) (1972) 1190–1194.

[6] A.M. Tarakhovskii, G.V. Glinskii, V.A. Shliakhovenko, Superoxide dismutase activity in tumor and liver of tumor-bearing animals, Ukr. Biokhim. Zh. 52 (5) (1980) 628–631.

[7] M. Mayerhofer, K.V. Gleixner, J. Mayerhofer, G. Hoermann, E. Jaeger, K.J. Aichberger, R.G. Ott, K. Greish, H. Nakamura, S. Derdak, P. Samorapoompichit, W.F. Pickl, V. Sexl, H. Esterbauer, I. Schwarzinger, C. Sillaber, H. Maeda, P. Valent, Targeting of heat shock protein 32 (Hsp32)/heme oxygenase-1 (HO-1) in leukemic cells in chronic myeloid leukemia: a novel approach to overcome resistance against imatinib, Blood 111 (4) (2008) 2200–2210.

[8] J. Fang, T. Sawa, T. Akaike, T. Akuta, S.K. Sahoo, G. Khaled, A. Hamada, H. Maeda, In vivo antitumor activity of pegylated zinc protoporphyrin: targeted inhibition of heme oxygenase in solid tumor, Cancer Res. 63 (13) (2003) 3567–3574.

[9] S.K. Sahoo, T. Sawa, J. Fang, S. Tanaka, Y. Miyamoto, T. Akaike, H. Maeda, Pegylated zinc protoporphyrin: a water-soluble heme oxygenase inhibitor with tumor-targeting capacity, Bioconjug. Chem. 13 (5) (2002) 1031–1038.

[10] H.W. Hwang, J.R. Lee, K.Y. Chou, C.S. Suen, M.J. Hwang, C. Chen, R.C. Shieh, L.Y. Chau, Oligomerization is crucial for the stability and function of heme oxygenase-1 in the endoplasmic reticulum, J. Biol. Chem. 284 (34) (2009) 22672–22679.

[11] A.K. Iyer, K. Greish, J. Fang, R. Murakami, H. Maeda, High-loading nanosized micelles of copoly(styrene-maleic acid)-zinc protoporphyrin for targeted delivery of a potent heme oxygenase inhibitor, Biomaterials 28 (10) (2007) 1871–1881.

[12] K. Greish, A. Nagamitsu, J. Fang, H. Maeda, Copoly(styrene-maleic acid)-pirarubicin micelles: high tumor-targeting efficiency with little toxicity, Bioconjug. Chem. 16 (1) (2005) 230–236.

[13] J. Fang, T. Sawa, T. Akaike, H. Maeda, Tumor-targeted delivery of polyethylene glycol-conjugated D-amino acid oxidase for antitumor therapy via enzymatic generation of hydrogen peroxide, Cancer Res. 62 (11) (2002) 3138–3143.

[14] J.J. Shiah, Y. Sun, C.M. Peterson, J. Kopecek, Biodistribution of free and N-(2-hydroxypropyl)methacrylamide copolymer-bound mesochlorin e(6) and adriamycin in nude mice bearing human ovarian carcinoma OVCAR-3 xenografts, J. Control. Release 61 (1–2) (1999) 145–157.

[15] Y. Matsumura, H. Maeda, A new concept for macromolecular therapeutics in cancer chemotherapy: mechanism of tumoritropic accumulation of proteins and the antitumor agent smancs, Cancer Res. 46 (12 Pt 1) (1986) 6387–6392.

[16] H. Maeda, T. Sawa, T. Konno, Mechanism of tumor-targeted delivery of macromolecular drugs, including the EPR effect in solid tumor and clinical overview of the prototype polymeric drug SMANCS, J. Control. Release 74 (1–3) (2001) 47–61.

[17] H. Maeda, Nitroglycerin enhances vascular blood flow and drug delivery in hypoxic tumor tissues: analogy between angina pectoris and solid tumors and enhancement of the EPR effect, J Control Release 142 (3) (2010) 296–298.

[18] H. Maeda, G.Y. Bharate, J. Daruwalla, Polymeric drugs for efficient tumor-targeted drug delivery based on EPR-effect, Eur. J. Pharm. Biopharm. 71 (3) (2009) 409–419.

[19] G. Gregoriadis, E.D. Neerunjun, Treatment of tumour bearing mice with liponsome-entrapped actinomycin D prolongs their survival, Res. Commun. Chem. Pathol. Pharmacol. 10 (2) (1975) 351–362.

[20] O. Hovorka, T. Etrych, V. Subr, J. Strohalm, K. Ulbrich, B. Rihova, HPMA based macromolecular therapeutics: internalization, intracellular pathway and cell death depend on the character of covalent bond between the drug and the peptidic spacer and also on spacer composition, J. Drug Target. 14 (6) (2006) 391–403.

[21] K. Sasaki, K. Kogure, S. Chaki, Y. Kihira, M. Ueno, H. Harashima, Construction of a multifunctional envelope-type nano device by a SUV*-fusion method, Int. J. Pharm. 296 (1–2) (2005) 142–150.

[22] C. Allen, Y. Yu, A. Eisenberg, D. Maysinger, Cellular internalization of PCL(20)-b-PEO (44) block copolymer micelles, Biochim. Biophys. Acta 1421 (1) (1999) 32–38.

[23] P. Lemieux, M. Page, C. Noel, In vivo cytotoxicity and antineoplastic activity of a transferrin-daunorubicin conjugate, In Vivo 6 (6) (1992) 621–627.

[24] P. van der Sluijs, H.P. Bootsma, B. Postema, F. Moolenaar, D.K. Meijer, Drug targeting to the liver with lactosylated albumins: does the glycoprotein target the drug or is the drug targeting the glycoprotein? Hepatology 6 (4) (1986) 723–728.

[25] C.P. Leamon, I. Pastan, P.S. Low, Cytotoxicity of folate-Pseudomonas exotoxin conjugates toward tumor cells. Contribution of translocation domain, J. Biol. Chem. 268 (33) (1993) 24847–24854.

[26] G.T. Colbern, D.J. Dykes, C. Engbers, R. Musterer, A. Hiller, E. Pegg, R. Saville, S. Weng, M. Luzzio, P. Uster, M. Amantea, P.K. Working, Encapsulation of the topoisomerase I inhibitor GL147211C in pegylated (STEALTH) liposomes: pharmacokinetics and antitumor activity in HT29 colon tumor xenografts, Clin. Cancer Res. 4 (12) (1998) 3077–3082.

[27] Y. Matsumura, T. Oda, H. Maeda, General mechanism of intratumor accumulation of macromolecules: advantage of macromolecular therapeutics, Gan To Kagaku Ryoho. 14 (3 Pt 2) (1987) 821–829.

[28] H. Maeda, J. Takeshita, R. Kanamaru, A lipophilic derivative of neocarzinostatin. A polymer conjugation of an antitumor protein antibiotic, Int. J. Pept. Protein Res. 14 (2) (1979) 81–87.

[29] K.A. Nieforth, R. Nadeau, I.H. Patel, D. Mould, Use of an indirect pharmacodynamic stimulation model of MX protein induction to compare in vivo activity of interferon alfa-2a and a polyethylene glycol-modified derivative in healthy subjects, Clin. Pharmacol. Ther. 59 (6) (1996) 636–646.

[30] T.M. Allen, C. Hansen, F. Martin, C. Redemann, A. Yau-Young, Liposomes containing synthetic lipid derivatives of poly(ethylene glycol) show prolonged circulation half-lives in vivo, Biochim. Biophys. Acta 1066 (1) (1991) 29–36.

[31] H. Maeda, Tumor-selective delivery of macromolecular drugs via the EPR effect: background and future prospects. Bioconjug Chem 21(5) 797–802.

[32] T. Masuda, H. Akita, K. Niikura, T. Nishio, M. Ukawa, K. Enoto, R. Danev, K. Nagayama, K. Ijiro, H. Harashima, Envelope-type lipid nanoparticles incorporating a short PEG-lipid conjugate for improved control of intracellular trafficking and transgene transcription, Biomaterials 30 (27) (2009) 4806–4814.

[33] H. Hatakeyama, H. Akita, K. Kogure, M. Oishi, Y. Nagasaki, Y. Kihira, M. Ueno, H. Kobayashi, H. Kikuchi, H. Harashima, Development of a novel systemic gene delivery system for cancer therapy with a tumor-specific cleavable PEG-lipid, Gene Ther. 14 (1) (2007) 68–77.

[34] T. Oda, F. Sato, H. Maeda, Facilitated internalization of neocarzinostatin and its lipophilic polymer conjugate, SMANCS, into cytosol in acidic pH, J Natl Cancer Inst 79 (6) (1987) 1205–1211.

[35] T. Oda, H. Maeda, Binding to and internalization by cultured cells of neocarzinostatin and enhancement of its actions by conjugation with lipophilic styrene-maleic acid copolymer, Cancer Res. 47 (12) (1987) 3206–3211.

[36] M. Regehly, K. Greish, F. Rancan, H. Maeda, F. Bohm, B. Roder, Water-soluble polymer conjugates of ZnPP for photodynamic tumor therapy, Bioconjug. Chem. 18 (2) (2007) 494–499.

[37] H. Xu, Y. Deng, D. Chen, W. Hong, Y. Lu, X. Dong, Esterase-catalyzed dePEGylation of pH-sensitive vesicles modified with cleavable PEG-lipid derivatives, J. Control. Release 130 (3) (2008) 238–245.

Journal of Drug Targeting, 2011; 19(10): 954–966

ISSN 1061-186X print/ISSN 1029-2330 online
DOI: 10.3109/1061186X.2011.633260

informa
healthcare

RESEARCH ARTICLE

4-Amino-6-hydroxypyrazolo [3,4-d]pyrimidine (AHPP) conjugated PEG micelles: Water soluble polymeric xanthine oxidase inhibitor

Gahininath Y. Bharate[1,2], Jun Fang[1], Hideaki Nakamura[1], Haibo Qin[1], Seiji Shinkai[2], and Hiroshi Maeda[1,2]

[1]Drug Delivery System Research Institute, Faculty of Pharmaceutical Sciences, and [2]Department of Nanoscience and Applied Chemistry, Graduate School of Engineering, Sojo University, Ikeda, Kumamoto, Japan

Abstract

Xanthine oxidase (XO) is the major source of superoxide anion (O_2^-) that is associated with various reactive oxygen species (ROS) related diseases. 4-amino-6-hydroxypyrazolo[3,4-d]pyrimidine (AHPP) is a potent XO inhibitor discovered in Maeda's laboratory, which is now being developed for the treatment of ischemia reperfusion injury and inflammatory diseases. However, the poor aqueous solubility of AHPP at physiological pH hampers its clinical development. To overcome this drawback, in the present study water soluble polyethyleneglycol conjugated AHPP (AHPP-PEG) was synthesized via two different approaches, which resulted in two derivatives of AHPP-PEG, namely, mono-AHPP-PEG and bis-(AHPP)-PEG depending on the number of AHPP on PEG chain. We characterized both conjugates by UV, FTIR spectroscopy and elemental analysis. Dynamic light scattering and Sephadex G-100 chromatography studies revealed mean particle size of 164.1 and 218.8 nm and Mw. equivalent to 107 and 126 kDa for mono-AHPP-PEG and bis-(AHPP)-PEG, respectively. Further, XO inhibitory activity for mono-AHPP-PEG and bis-(AHPP)-PEG were found with Ki of 0.23 ± 0.03 and 0.21 ± 0.03 μM, respectively. *In vivo* pharmacokinetic study showed longer circulation time of AHPP-PEG conjugates compared to free AHPP. These results indicate AHPP-PEG conjugates have better potentials with supramolecular assemblies in aqueous medium and may become a good candidate for the treatment of ROS related diseases.

Keywords: Pharmacokinetics, superoxide anion, xanthine oxidase, AHPP, inflammation targeted, cytoprotection

Introduction

Xanthine oxidase (XO) is known to exist in many tissues including heart and they catalyses the two-step oxidation of hypoxanthine (Figure 1), from hypoxanthine to xanthine, and then xanthine to uric acid (Cappola et al. 2001; Freehold et al. 1972; Feigelson et al. 1957). XO is well known as a major enzyme to generate superoxide anion ($O_2^{\bullet-}$) that is a major type of reactive oxygen species (ROS) involved in many diseases and disorders, including damaged tissues as well as in the vascular system (Adachi et al. 1993; Jarasch et al. 1981; Jarasch et al. 1986; Oates et al. 2001; Pacher et al. 2006). Moreover, superoxide anion radical ($O_2^{\bullet-}$) immediately reacts with nitric oxide (NO) at diffusion dependent velocity to form more toxic peroxynitrite ($ONOO^-$), which is principally involved in the pathogenesis of various inflammatory disorders including viral and bacterial infections (Oda et al. 1989; Huie et al. 1993; Radi et al. 1991; Crow et al. 1995; Gryglewski et al. 1986; Moncada et al. 1991). In this connection, we previously verified that inhibition of xanthine oxidase resulted in the prolongation of biologic $t_{1/2}$ of NO *in vivo*, which consequently resulted in the lowering of blood pressure.

Thus, inhibiting XO may become a therapeutic to many diseases including inflammation and hypertension. Among inhibitors of XO, allopurinol is used in

Address for Correspondence: Prof. Hiroshi Maeda, Laboratory of Microbiology and Oncology, Faculty of Pharmaceutical Sciences, Sojo University, Ikeda 4-22-1, Kumamoto, 860 0082, Japan. Tel/Fax: +81-96-326-4114. E-mail: hirmaeda@ph.sojo-u.ac.jp

(Received 11 September 2011; revised 15 October 2011; accepted 16 October 2011)

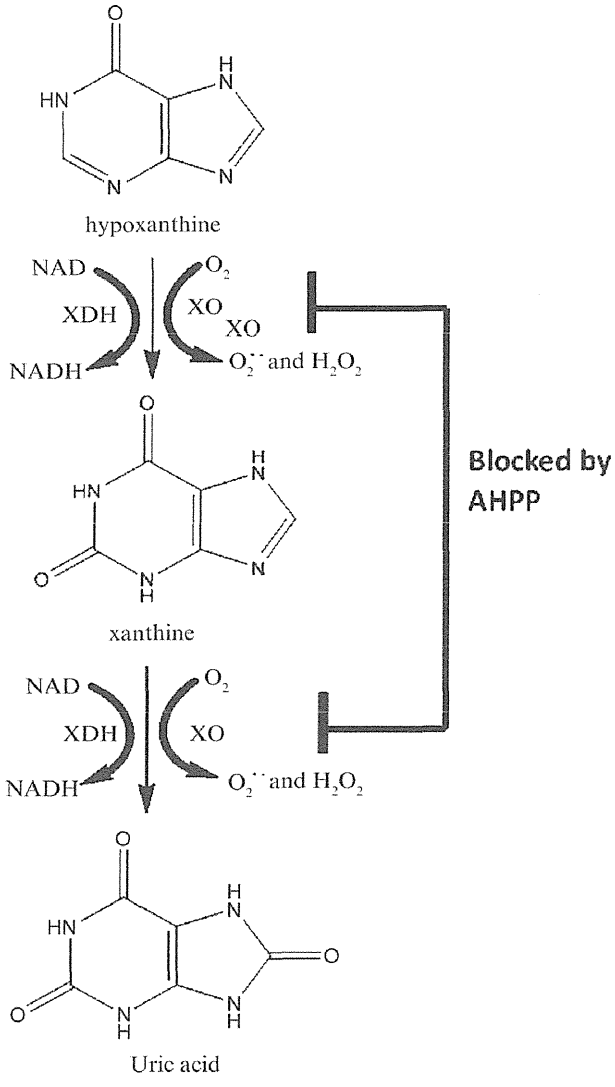

Figure 1. The degradation pathway of purine. XO catalyze the oxidation of hypoxanthine to xanthine and further catalyze the oxidation of xanthine to uric acid. This enzyme plays important role in catabolism of purine. In the reaction of xanthine to uric acid, an oxygen atom is transferred from molyobdenum to xanthine.

clinic for the treatment of hyperuricemia, but the effect of allopurinol is not dose-dependent, at higher dose it becomes substrate of XO (Miyamoto et al. 1996). Recently, we developed 4-amino-6-hydroxypyrazolo [3,4-d] pyrimidine (AHPP), one of the pyrazolopyrimidine derivatives that has exhibited potent XO inhibitory activity. However, AHPP *per se* shows poor aqueous solubility, which prevents clinical development. To overcome this drawback in the current study, we synthesized two water-soluble conjugates of AHPP (4-amino-6-hydroxypyrazolo [3,4-d] pyrimidine) with PEG (polyethyleneglycol).

In addition, the present AHPP-PEG conjugates are designed to exhibit macromolecular nature and thus showed longer plasma half-life and selectively accumulation in inflammatory tissues by taking advantage of the enhanced vascular permeability and retention (EPR) effect (Matsumura et al. 1986; Maeda et al. 2001a, 2001b). Thus, AHPP-PEG conjugates may become a new candidate for ROS related diseases such as inflammatory disease. In this study, the synthesis and characterization of AHPP-PEG were investigated. The *in vivo* pharmacokinetics was also discussed.

Materials and experimental methods

Materials

Poly(oxy-1,-2-ethanediyl)-α-methyl-ω-[2-[(2,5-dioxopyrrolidinyl)oxy]-2-oxoethyoxy]-PEG (Sunbright ME-020AS; Mw 2280; PDI 0.2) was obtained from NOF Corp., Tokyo, Japan. 4-amino-6-hydroxypyrazolo- [3,4-d] pyrimidine (AHPP), xanthine, polyethylene glycol (mean Mn, 2000), 4-phenylspiro[furan-2(3H)-1′-phthalan]-3,3′-dione (fluorescamine), 2,4,6-trinitrobenzenesulfonic acid (TNBS), trichloroacetic acid and other reagents of reagent grade, were purchased from Wako Pure Chemical Industries (Osaka) and were used without further purification. 4-nitrophenyl chloroformate, Bovine milk xanthine oxidase (XO) was purchased from Sigma-Aldrich Chemical Co, (St Louis, MO, USA). AHPP and xanthine solutions were prepared by dissolution in 0.25 M NaOH at a concentration of 0.1 M and were diluted to appropriate concentration with distilled water or physiological saline. All other solvents and chemical reagents were purchased from commercial sources and used without further purification.

Experimental methods

Synthesis of mono-AHPP-PEG conjugated micelles

As depicted in the reaction Scheme 1, 100 mg (0.661 mmol) of 4-amino-6-hydroxypyrazolo [3,4-d] pyrimidine (AHPP) was first dissolved in 15 mL of 0.1 M NaOH solution at room temperature, under stirring for 15 min. Then the solution was cooled to 0–4°C, 1.322 g (0.661 mmol) of poly(oxy-1, 2-ethanediyl)-α-methyl-ω-[2-(2,5-dioxopyrrolidinyl)oxy]-2-oxoethyoxy]-PEG (PEG ME-20AS, NOF Corp.) in 20 mL chloroform was added drop wise for 40 min at 4°C with vigorous stirring. When the addition of PEG was completed the reaction mixture was vigorously stirred for next 2 h at 4°C. The reaction between two components in two layers will undergo as interfacial conjugation reaction under vigorous stirring. Then, the chloroform layer containing the final product (lower layer) was separated by using separating funnel. Chloroform was removed by using a rotary evaporator in vacuum and the conjugate was precipitated by addition with acetone. The resultant viscous product was then dissolved in 40 mL deionized water and lyophilized to obtain fluffy colorless product of mono-AHPP-PEG, conjugate (1.23 g; 87% based on AHPP). By addition of about 50 mL of water to mono-AHPP-PEG, it was readily